A Model of Tidal Rectification by Potential Vorticity Mixing. Part II: Frontal Regime*

HSIEN-WANG OU

Lamont-Doherty Earth Observatory of Columbia University, Palisades, New York

ABSTRACT

A model of tidal rectification in a homogeneous ocean (Part I) is extended here to include a front that separates shelf and slope waters. The front is approximated as a density discontinuity, the stratification and anchoring position of which are given, but which otherwise is coupled to the flow field. The dynamical closure is formulated through vorticity balance of the two layers and a parameterization of potential vorticity (PV) flux in terms of local tidal amplitude and the mean field.

As an example of the frontal effect on the tidally rectified flow, a solution is calculated for the case of negligible interfacial stress and PV flux in the bottom boundary layer and compared with that of a homogeneous ocean. It is found that the mean along-isobath flow outside the frontal zone remains largely unchanged, but is qualitatively altered in the frontal zone. Specifically, the mean flow above the sloping front—being insulated from bottom friction—is greatly intensified by PV mixing, consistent with observed seasonal change over Georges Bank. The mean flow below the frontal interface on the other hand is weakened by enhanced frictional effect— to nearly zero at the foot of the front. The vanishing Ekman transport would strengthen the front as a barrier to offshore transport of a passive tracer.

1. Introduction

This is Part II of a two-part paper motivated by the clockwise gyre observed over Georges Bank off the northeastern Unites States. Although the gyre is intensified in summer—as one would expect from thermal-wind balance, it is prominent even in winter when the stratification is absent. This latter feature, in particular, has been attributed to tidal rectification, a proposition that has received strong support from both modeling and observational studies. Previous explanations of the rectification mechanism (Loder 1980) have invoked bottom friction as the source of the tidal flux—hence referred as "friction" mechanism. But drawing analogy from tidal dispersion of passive tracers, I have proposed a different "diffusivity" mechanism based on horizontal mixing of potential vorticity (PV).

In Part I (Ou 1999), a homogeneous ocean is considered to elucidate the diffusivity mechanism, and to contrast it with the previous friction mechanism. While both mechanisms produce a mean flow of the right direction, the functional dependence of its strength on

tidal amplitude is notably different. In a typical regime when the mean shear is small compared with the Coriolis parameter, this dependence is quadratic for the friction mechanism, but linear for the diffusivity mechanism. This latter dependence compares more favorably with observations over the northern slope of Georges Bank (Magnell et al. 1980), lending support to the diffusivity mechanism.

Common to both mechanisms, however, the mean flow is proportional to the underlying topographic slope. Combined with its increase with local tidal amplitude, the rectified flow thus attains a maximum near the shelf break. Over the Georges Bank, this is also a region where there is a prominent front in summer when the gyre is most intense. To examine this seasonal effect, and for a closer comparison with observation, one needs to include a front in the model, which motivates the present study.

Tidal rectification in a stratified ocean has been considered previously. Loder and Wright (1985) extended Loder's (1980) homogeneous model to include a front, the density field of which is specified. Since the along-isobath flow is dominated by the baroclinic component in the frontal zone, the fixation of the density field has limited the prognostic utility of the model. In numerical models, on the other hand, this important coupling of density to the flow fields has been retained. In a two-dimensional model of the Georges Bank (on a vertical plane normal to depth contours), Chen and Beardsley (1995) considered the evolution of the density and flow

---

Corresponding author address: Dr. Hsien-Wang Ou, Lamont-Doherty Earth Observatory of Columbia University, Route 9W, Palisades, NY 10964.
E-mail: dou@ldeo.columbia.edu

fields when an initial uniform stratification is subject to tidal forcing. Strong tidal mixing over the top of the bank renders the water there homogeneous, which is separated from the offshore stratification—largely unchanged from the initial condition—through a frontal zone of sloping density surfaces. When compared with the solution of a homogeneous ocean, the maximum flow induced by tidal rectification has doubled in strength. In three-dimensional models of Georges Bank, Namie (1996) found that, when density is a prognostic variable, the tide-induced mean flow is substantially stronger than in the case when the density field is prescribed from climatic data. This enhanced flow compares more favorably with observation, underscoring the importance of a density field that is interactive with the flow field.

As these numerical models have used primitive equations, they have contained, to some degree, the diffusivity mechanism arising from the tidal random walk. But because of complication of the numerical models, it is difficult to discern the dominant balances that govern the rectified flow in a frontal regime. As a natural extension to Part I, I therefore consider here the tidal rectified flow when there is a bottom-to-surface front, approximated as a density discontinuity. As the front is taken as a given fact, the model obviously may not address important questions related to frontogenesis. Its objectives are simply to formulate the dynamical closure of such a system based on a diffusivity parameterization and to examine how the solution of a homogeneous ocean may be modified. For organization of the paper, I discuss in section 2 the model formulation and the governing equations. In section 3, these equations are further simplified, and a solution is obtained to illustrate qualitative effects of the front. The paper is concluded with additional discussion in section 4.

2. Model

As discussed above, it is essential for the study of tidal rectification that the depth of the frontal interface be coupled dynamically to the flow field. But other properties of the front are taken as given here since they depend also on processes external to tidal rectification. For example, we are not inquiring about buoyancy balance, which determines density difference across the front, or the mechanical energy balance, which constrains its anchoring depth, both of which are therefore taken as external parameters for the present study.

To simplify the calculation later, the topography is considered a straight submarine bank symmetric about its axis. This topography is slightly different from that used in Part I, which comprises of a slope flanked by flat bottoms extending to the far field in both directions. But, since the boundary condition to be imposed at the bank axis is the vanishing of mean flow and PV flux—same as that for the far field of Part I, the two solutions can be compared. Because of symmetry, one needs only
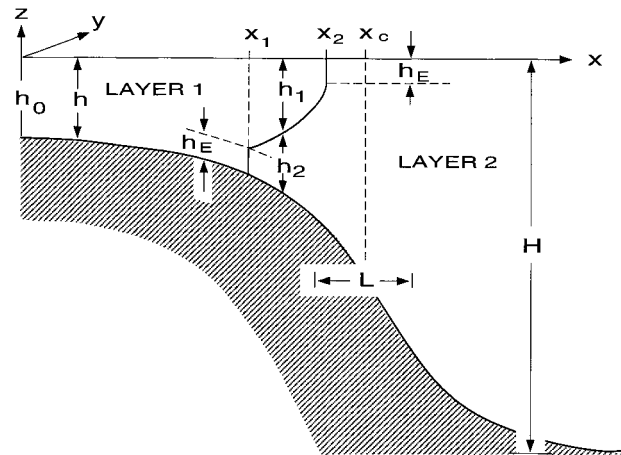

FIG. 1. The model domain, which covers one flank of a straight submarine bank symmetric about its axis. The depth profile is that of a hyperbolic tangent centered at x_c with an e-folding width of L. There is a density front that extends from bottom to surface, and frictional boundary layers of thickness h_E abutting the bottom and surface within which the front is vertical.

to consider one flank of the bank, as shown schematically in Fig. 1. A right-handed Cartesian coordinate system is used with x, y, and z axes directed offshore, along-isobath, and upward, respectively. The origin is set over the bank axis, and x_1 and x_2 mark where the front intersects the bottom and the surface, respectively. For the present convention, variables for the inshore and offshore water masses will be tagged by a subscript j ($=1$, 2), and their values at x_1 and x_2 by a second subscript i ($=1$, 2), respectively.

As in Part I, the model is forced only by cross-isobath tidal current. Although there is now an internal tide because of stratification, observations (Brickman and Loder 1993) suggest that the internal tide is highly intermittent, with an average energy level one or two orders lower than that of the barotropic tide. For simplicity, the internal tide is thus neglected. If one denotes the water depth by h and the amplitude of tidal current by U, the continuity equation implies then

$$hU = HU_\infty, \qquad (2.1)$$

where H and U_∞ are respective values of h and U in the far field. As indicated in Fig. 1, I have appended frictional boundary layers abutting the bottom and surface within which the front is vertical, and the thickness of which—the Ekman depth h_E—is taken as given. Since we have underscored the importance of bottom friction in Part I, it is only logical to include a finite frictional boundary layer, which is a prominent feature in the frontal zone (Houghton 1997). Moreover, as we shall see later, friction enters the vorticity balance through a stress divided by layer thickness, the finiteness of the layer thickness is thus needed to avoid singularities.

We have demonstrated in Part I the central role of vorticity balance in determining the mean flow. With

primed and overbarred variables denoting fluctuating and tide-averaged components respectively, this balance can be expressed symbolically as

$$dF/dx = d\tau/dx, \tag{2.2}$$

where

$$F = h\overline{u'q'} \tag{2.3}$$

is the PV flux and

$$\tau = -C_D U\overline{v}/h \tag{2.4}$$

is the bottom stress divided by water depth. In above equations, u and v are the two velocity components, q the potential vorticity, and C_D a constant drag coefficient. Because of symmetry, both F and τ vanish at the bank axis so that (2.2) can be integrated once to yield

$$F = \tau, \tag{2.5}$$

which relates PV flux to the local stress.

In the stratified model considered here, τ in (2.2) includes the interfacial stress acting on the sloping part of the front and the equation must be expanded to include PV flux across the vertical portion of the front (i.e., within the frictional boundary layers). To express it symbolically, we have then, for layer 1 (the inshore water mass),

$$dF_1/dx = d\tau_1/dx - F_{2,1}\delta(x - x_1), \tag{2.6}$$

where $F_{2,1}$ is the PV flux of layer 2 evaluated at x_1 and δ is the Kronecker delta function signifying that such a flux acts like a point source for layer 1. Since a positive $F_{2,1}$ (i.e., an offshore PV flux) implies a loss of PV from the inshore water, there is thus a negative sign before this flux. By symmetry, we have again

$$F_1 = \tau_1 = \overline{v}_1 = 0 \quad \text{at } x = 0 \tag{2.7}$$

so that (2.6) may be integrated once to yield

$$F_1 = \tau_1 - F_{2,1}\Gamma(x - x_1), \tag{2.8}$$

where Γ is the Heaviside step function with the argument $x - x_1$. Inshore of the frontal zone ($x < x_1$), $\Gamma = 0$ and τ_1 is due solely to the bottom stress,

$$\tau_1 = -C_D U\overline{v}_1/h \quad \text{for } x < x_1. \tag{2.9}$$

Equation (2.8) thus reduces to that of a homogeneous ocean (2.5). In the frontal zone ($x_1 < x < x_2$) however, $\Gamma = 1$, so the PV flux above the front is decreased by that lost through the vertical front at x_1; since layer 1 now overlies an interface, τ_1 is due solely to the interfacial stress. Drawing an analogy with the bottom stress, this interfacial stress can be written as (see, e.g., Csanady 1982)

$$\tau_1 = -C_I U(\overline{v}_1 - \overline{v}_2)/\overline{h}_1 \quad \text{for } x_1 < x < x_2, \tag{2.10}$$

where $\overline{h}_1$, a prognostic variable, is the depth of the upper layer and C_I is an interfacial drag coefficient taken as external, the value of which remains unspecified at the moment. One notes that, since both terms on the rhs of

(2.8) are discontinuous at x_1, so is the PV flux F_1. This is to be expected given the model approximations, which however has no bearing on the well-posedness of the problem. But to maintain finiteness of PV and PV flux, v_1 and q_1 must be continuous across x_1—despite the discontinuity in the upper-layer depth. Applying (2.8) at x_2, one then has

$$F_{1,2} = \tau_{1,2} - F_{2,1}, \tag{2.11}$$

or the PV flux across the outcrop x_2 (lhs) has two sources: the net torque acting on the surface layer, which depends only on the interfacial stress at x_2, and influx of PV across the vertical front at x_1.

Now let us consider the corresponding equations for the lower layer. The counterpart to (2.6) is

$$dF_2/dx = d\tau_2/dx + F_{1,2}\delta(x - x_2), \tag{2.12}$$

where $F_{1,2}$ is the PV flux of layer 1 at x_2 that appears in (2.11). As this is the influx of PV into layer 2, the sign before the term is now positive. Since in the far field,

$$F_2, \tau_2, \overline{v}_2 \to 0 \quad \text{as } x \to \infty, \tag{2.13}$$

(2.12) may be integrated once to yield

$$F_2 = \tau_2 - F_{1,2}\Gamma(x_2 - x). \tag{2.14}$$

Again, outside the frontal zone ($x > x_2$), τ_2 is due solely to the bottom stress,

$$\tau_2 = -C_D U\overline{v}_2/h \quad \text{for } x > x_2, \tag{2.15}$$

and $\Gamma = 0$; (2.14) is as given for the homogeneous ocean. But within the frontal zone ($x_1 < x < x_2$), $\Gamma = 1$, so the PV flux below the front must be altered by that across the surface front—in order for the PV flux to vanish in the far field. Since the lower layer in the frontal zone is sandwiched between the sloping interface and bottom, τ_2 contains both interfacial and bottom stresses, or

$$\tau_2 = C_I U(\overline{v}_1 - \overline{v}_2)/\overline{h}_2 - C_D U\overline{v}_2/\overline{h}_2$$
$$\text{for } x_1 < x < x_2, \tag{2.16}$$

where $\overline{h}_2$ is the depth of the lower layer, which is related to that of the upper layer by

$$\overline{h}_1 + \overline{h}_2 = h. \tag{2.17}$$

Again, if one applies (2.14) at x_1, one obtains

$$F_{2,1} = \tau_{2,1} - F_{1,2}, \tag{2.18}$$

which is the counterpart to (2.11).

The formulation so far is independent of tidal rectification, which enters only when one tries to link PV fluxes to the mean field. In Part I, I draw the analogy between tidal mixing of PV and that of passive tracers in arguing that the tidal flux of PV can be parameterized through a tidal diffusivity. In the present notation, one has then, for layer j,

$$F_j = -\kappa \overline{h}_j d\overline{q}_j/dx, \tag{2.19}$$

where

$$\overline{q}_j = \overline{h}_j^{-1}(f + d\overline{v}_j/dx) \qquad (2.20)$$

is the mean PV with f being the Coriolis parameter, and

$$\kappa = bUl \qquad (2.21)$$

is tidal diffusivity, with b being a mixing coefficient, the magnitude of which is assumed independent of the tidal amplitude, and l the local tidal excursion. Having expressed F_j and τ_j in terms of the mean flow $\overline{v}_j$, Eqs. (2.8) and (2.14) constitute a pair of ordinary differential equations governing $\overline{v}_j$. When compared with that of the homogeneous ocean, they contain additional degrees of freedom associated with unknown internal fluxes $F_{2,1}$, $F_{1,2}$ and the mean interfacial depth $\overline{h}_1$. The former two are constrained by the requirements (2.11) and (2.18), and the variable $\overline{h}_1$ is coupled to the flow field through Margules equation,

$$f(\overline{v}_1 - \overline{v}_2) = g'd\overline{h}_1/dx, \qquad (2.22)$$

where g' is the reduced gravity. In writing (2.22), it is important to note that we have not assumed the flow to be geostrophic, but merely that tidal stresses in the interior do not have vertical structure, which is a consequence of the neglect of internal tide. Given the anchoring depth of the front, the interfacial depth is thus uniquely specified by the flow field and, hence, does not require additional constraints for its determination. Given that Eqs. (2.8) and (2.14) are of second order in the $\overline{v}_j$, one thus needs two more conditions besides (2.7) and (2.13) to close the problem. These are provided by parameterizing PV fluxes $F_{2,1}$ and $F_{1,2}$ in terms of the mean field. In parallel with that in the interior, we express

$$F_{2,1} = -\kappa_1 h_E[\overline{q}_2 - \overline{q}_1]_{,1} \qquad (2.23)$$

and

$$F_{1,2} = -\kappa_2 h_E[\overline{q}_2 - \overline{q}_1]_{,2}, \qquad (2.24)$$

where κ_1 and κ_2 are transfer coefficients across the bottom and surface fronts, respectively. These coefficients will be related to local tidal amplitude later, but may remain unspecified at the present. With coefficients κ, κ_1, κ_2, and C_I taken as given, the problem is thus closed. To see this closure more clearly, one may integrate Eqs. (2.8), (2.14), and (2.22) from $x = 0$ forward to the far field, and inquire how many unknown values need to be guessed along the way, and whether that number matches the number of independent constraints. To initiate the integration from $x = 0$, one needs to guess the value of $\overline{q}_1$ since $\overline{v}_1 = 0$ at the origin. After reaching x_1, one needs to guess the values of $F_{2,1}$ [which through (2.23) also fixes $\overline{q}_2$], $\overline{v}_2$, and $F_{1,2}$ to proceed further. After reaching x_2 (i.e., where $\overline{h}_1 = h_E$), one may continue on to the far field without additional guesses. There are therefore in total four degrees of freedom, and the four independent constraints needed to close the problem are (2.11), (2.13), (2.18), and (2.24). Note that the

condition (2.23) has already been used in the above integration. While the above procedure serves to illustrate closure of the problem, it is not yet practical for obtaining the solution since it contains too many degrees of freedom (i.e., one has to guess a point in a four-dimensional parameter space).

To further simplify the problem, I shall first replace net PV balances of the inshore and offshore water masses [i.e., (2.11) and (2.18)] by those of the inshore water mass and the frontal system as a whole but expressed explicitly in terms of the mean fields. If one subtracts (2.18) from (2.11), and removes the common factor h_E, the PV balance of the system as a whole is obtained, which is given by

$$\underset{>0}{-[C_IU(\overline{v}_1 - \overline{v}_2)]_{,2}} \ \underset{>0}{- [C_IU(\overline{v}_1 - \overline{v}_2)]_{,1}} \ \underset{<0}{+ [C_DU\overline{v}_2]_{,1}}$$

$$= 0. \qquad (2.25)$$

This equation states that, since there is no PV flux entering the system, the net torque acting on the whole system must vanish. This torque consists of that acting on the upper layer (the first term) and that acting on the lower layer (the last two terms), noting that bottom stress vanishes at $x = 0$ and the far field. One notes that, since the PV fluxes across the vertical front at x_1 and x_2 only redistribute PV within the frontal system, they do not enter the above balance. I have also indicated the plausible sign of the terms by noting that the frontal interface generally slopes upward offshore. Through the thermal-wind relation, the current shear across the sloping front is thus negative, or the interfacial stress tends to increase the vorticity of the system. For the balance to hold, $\overline{v}_{2,1}$—the lower-layer flow just offshore of the bottom front—thus must be negative in order for the bottom torque to counter the interfacial torque. How strong this flow needs to be depends on relative importance of the interfacial to bottom drag coefficient, which will be discussed further in section 3. It is interesting to note that the first two terms may not balance each other, which underscores the importance of bottom friction in the closure.

The PV balance of the upper layer (2.11), when expressed in mean fields, is given by

$$\underset{<0}{h_E\kappa_2[\overline{q}_2 - \overline{q}_1]_{,2}} + \underset{>0}{h_E\kappa_1[\overline{q}_2 - \overline{q}_1]_{,1}} - \underset{>0}{[C_IU(\overline{v}_1 - \overline{v}_2)/h_E]_{,2}}$$

$$= 0, \qquad (2.26)$$

which states that PV fluxes into the upper layer through surface and bottom fronts (the first two terms, respectively) are balanced by the torque acting on the layer (the third term). Plausible signs of the three terms are also indicated based on the following reasoning: One may assume relative vorticity to be small compared with the Coriolis parameter so that PV value is dominated by its dependence on layer thickness. In such a case, the first term would be negative, or mixing across the

surface front between a thin upper layer and a thick offshore water column tends to decrease PV of the inshore water. By the same token, the second term is positive, or mixing across the bottom front between the wedged lower layer and thicker inshore water column tends to increase PV of the inshore water. Again, the thermal wind implies that the third term is positive or interfacial stress tends to exert a cyclonic torque on the upper layer. Since the second and third terms are of the same sign, the balance is possible only if the first term is retained, which thus underscores the importance of PV mixing across the surface front regardless of the magnitude of transfer and interfacial drag coefficients. This realization will be utilized in the next section for further simplification of the problem.

3. Solution

As we have remarked earlier, although the problem is demonstrably closed, the solution remains intractable because of the large number of degrees of freedom that hampers the numerical procedure. On the other hand, one notes that the problem contains coefficients such as C_I, κ_1, and κ_2, which do not have intrinsic values, but simply reflect the efficiency of exchange processes across the front. The variability of these processes undoubtedly contribute to variability of the frontal structure, and there is no justification that these parameters be assigned specific and precise values. Rather, to elucidate the qualitative effect of the front, I shall consider plausible ranges of these parameters that allow further simplification of the problem.

First, to highlight the difference from the homogeneous model, I shall consider the case of a strongly stratified front so that mixing across the sloping part of the front may be neglected. This is sensible since front is by definition where the mixing is curtailed—relative to the ambient water masses. In numerical models, vertical diffusivity and viscosity are often parameterized in terms of a Richardson number. Enhanced stratification across a frontal interface would increase the Richardson number, thus impeding vertical mixing. Tracer release experiments conducted near the New England shelf-break front in summer (Houghton 1997) have shown that tracer mostly disperses along the front rather then across the front, consistent with this assessment. With this reduced cross-frontal mixing applied to dynamical properties, one assumes then interfacial stress is negligible, and from the vorticity balance (2.25), one deduces then

$$\overline{v}_{2,1} \approx 0. \tag{3.1}$$

I have argued earlier that $\overline{v}_{2,1}$ is likely to be negative, and now with the neglect of the interfacial stress, this negative value is further argued to be near zero since the bottom torque associated with this flow constitutes the only vorticity sink of the system. This deduction (3.1) obviously is quite different from that of an inviscid

geostrophic adjustment (see, e.g., Csanady 1971) in which the bottom velocity is comparable to that at the surface. In the coastal environment, particularly where tidal current and hence bottom friction is important, one expects (3.1) to be more sensible, which indeed is more consistent with observation (Butman et al. 1982).

Another simplification concerns the neglect of PV flux across the bottom front, as justified below. If the instantaneous front is sufficiently sharp, one may assume that the tidally averaged front—the mean field of concern here—has a width scaled by the local tidal excursion. If the parameterization (2.19) is now applied to the vertical portion of the front, one derives that

$$F_{j,i} = -h_E b[Ul(\overline{q}_2 - \overline{q}_1)/l]_{,i} = -h_E b[U(\overline{q}_2 - \overline{q}_1)]_{,i}. \tag{3.2}$$

Comparing (3.2) with (2.23) and (2.24), one may relate the transfer coefficient to local tidal amplitude as

$$\kappa_i = bU_{,i}. \tag{3.3}$$

Since the amplitude of the tidal current is much reduced in the bottom boundary layer through which the flow is adjusted to no-slip at the boundary, one expects the transfer coefficient there to be small, which provides a justification for the neglect of the PV flux across the bottom front. Combined with the neglect of the interfacial stress, the vorticity balance of the upper layer (2.26) then reduces to

$$\overline{q}_2 \approx \overline{q}_1. \tag{3.4}$$

We have discussed earlier following the derivation of (2.26) that PV flux across the surface front must be important in that balance. Now with the vanishing of the other two terms in the equation, this PV flux must also vanish, which implies an equalization of PV across the surface front, given the finiteness of the transfer coefficient κ_2.

With the neglect of interfacial stress and PV flux across the bottom front, the governing equations (2.8) and (2.14) are also simplified—within the frontal zone. Equation (2.8) is now reduced to the statement that PV is homogenized above the front, the value of which—as seen from (3.4)—equals that just offshore of the surface front. Concomitantly, Eq. (2.14) is reduced to a balance between horizontal mixing and bottom torque, much like that for a homogeneous ocean except that the water depth in the latter case is now replaced by the thickness of the lower layer.

With these simplifications, one may now proceed to the derivation of the solution. To isolate the relevant dimensionless parameters on which the solution depends, I shall recast the governing equations in nondimensional form. Specifically, the layer thickness will be scaled by the water depth in the far field H, the horizontal distance by L that characterizes the scale of the topographic slope (more precisely defined later when a specific form of the topography is used), mean velocity by fL, and PV by f/H. If one defines the baroclinic

deformation radius as $R_c = (g'H)^{1/2}/f$, the Burger number as $B = (R_c/L)^2$, and a dimensionless friction coefficient as

$$\alpha = \frac{C_D L}{bH} \cdot \frac{L}{l_\infty}, \qquad (3.5)$$

then the governing equations can be given by, neglecting overbars for simplicity, for $x < x_1$:

$$\frac{dq_1}{dx} = \frac{\alpha}{h} \cdot v_1, \quad \text{and} \qquad (3.6)$$

$$\frac{dv_1}{dx} = q_1 h - 1; \qquad (3.7)$$

for $x_1 < x < x_2$:

$$\frac{dq_1}{dx} = 0, \qquad (3.8)$$

$$\frac{dv_1}{dx} = q_1 h_1 - 1, \qquad (3.9)$$

$$\frac{dq_2}{dx} = \frac{\alpha h}{h_2^2} \cdot v_2, \qquad (3.10)$$

$$\frac{dv_2}{dx} = q_2 h_2 - 1, \qquad (3.11)$$

$$\frac{dh_1}{dx} = \frac{1}{B} \cdot (v_1 - v_2), \qquad (3.12)$$

$$h_2 = h - h_1; \qquad (3.13)$$

and for $x_2 < x$:

$$\frac{dq_2}{dx} = \frac{\alpha}{h} \cdot v_2, \qquad (3.14)$$

$$\frac{dv_2}{dx} = q_2 h - 1. \qquad (3.15)$$

The boundary conditions are that given by (2.7), (3.1), (3.4), and (2.13):

$$v_1 = 0 \quad \text{at } x = 0, \qquad (3.16)$$

$$v_2 = 0 \quad \text{at } x = x_1, \qquad (3.17)$$

$$q_1 = q_2 \quad \text{at } x = x_2, \quad \text{and} \qquad (3.18)$$

$$v_2 \to 0 \quad \text{as } x \to \infty. \qquad (3.19)$$

The procedure for obtaining the numerical solution follows that discussed earlier regarding the closure of the problem, but now one needs to guess only two unknowns. Specifically, given (3.16), one needs to guess the value of q_1 to initiate the integration of (3.6) and (3.7). When reaching x_1 (an external parameter), one needs only to guess the value of q_2 to proceed with the integration of (3.8) through (3.13) since v_2 vanishes (3.17), and that q_1 and v_1 are continuous. The integration proceeds until $h_1 = h_E$, which defines x_2. Since q_2 and v_2 are continuous across x_2, (3.15) and (3.16) may then

be integrated forward to the far field. When reaching the far field, one may then check the constraints (3.18) and (3.19), and the initial guesses are adjusted until these constraints are satisfied. To facilitate integration to the far field set at an arbitrarily chosen large x, the grid spacing beyond x_2 is logarithmic. One may visualize the two constraints as two curves lying on a two-dimensional parameter space (spanned by the unknown values of $q_{1,0}$ and $q_{2,1}$), the intersection of which specifies the solution. For a systematic implementation of the procedure, one needs only to begin with a rectangular box that is sufficiently large that it encompasses the solution, and then halves its dimension at each iteration until the box is sufficiently small; that is, the constraints are satisfied to the desired accuracy.

From the governing equations, one sees that, besides the topography given by h, there are three external parameters: namely, x_1 that marks the anchor position of the front, the Burger number B that measures the stratification of the front, and the friction parameter α that measures the magnitude of the bottom friction—relative to the horizontal mixing. For illustrative purpose, I shall first present the solution for a typical set of values for these external parameters and then discuss how the solution would vary when these values are changed. The topography to be used is that of a hyperbolic tangent that varies smoothly from the bank top of depth h_0 to the far field of unit depth,

$$h = \gamma \tanh(x - x_c) + 1 - \gamma \qquad (3.20)$$

with

$$\gamma = (1 + \tanh x_c)^{-1}(1 - h_0). \qquad (3.21)$$

The center of the sloping region lies at x_c and its e-folding width is of unity (since it defines the scale of the horizontal distance). To determine representative values for the external parameters, let us set $g' = 0.5$ cm s^{-2}, $H = 200$ m, and $f = 10^{-4}$ s^{-1} to obtain baroclinic deformation radius of $R_c = 10$ km. The dimensional e-folding width of the sloping region is set to be the same; that is, $L = 10$ km so that the velocity scale is 1 m s^{-1} and the Burger number $B = 1$. To estimate α, I use in addition (see Part I) $C_D = 2 \times 10^{-3}$, $b = 0.1$, and $l_\infty = 2$ km to arrive at $\alpha = 5$. The Ekman layer thickness is set at 10 m, the depth of the bank top is 40 m, the midpoint of the sloping region and the anchor position of the front lie at a distance of $3L$ and $2L$ from the bank axis, respectively.

With these external values, the solution for the frontal interface (solid line) and velocities in the two layers (solid arrows) are plotted in Fig. 2. Also plotted is the velocity for the homogeneous ocean (dashed arrows) for comparison. Offshore of the frontal zone, the rectified flow remains largely unaffected by the presence of the front. The flow inshore of the frontal zone is also comparable to that of the homogeneous solution, but is slightly intensified. This is because mixing across the surface front has decreased PV of the inshore water [as
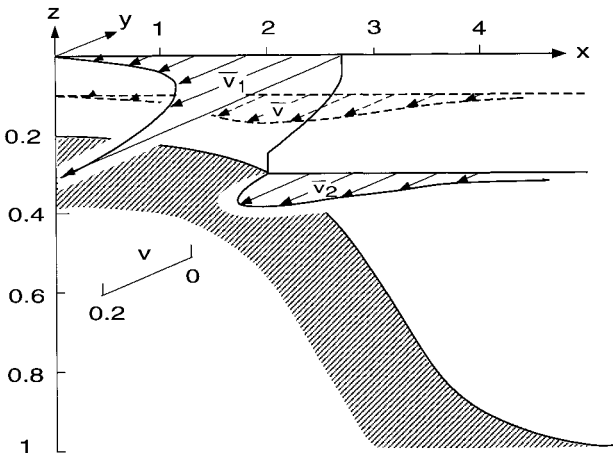
FIG. 2. The solution for the case of $x_c = 3$, $h_0 = 0.2$, $h_E = 0.05$, $x_1 = 2$, $B = 1$, and $\alpha = 5$. The solid line is the frontal interface, solid arrows indicate mean along-isobath velocities in the two layers, and dashed arrows the mean velocity for the homogeneous ocean.

entailed in the constraint (3.18)], thus enhancing the negative shear.

In the frontal zone, there is, on the other hand, a qualitative alteration of the flow field. As the fluid above the sloping front is insulated from bottom friction (through the neglect of the interfacial stress), PV above the front is homogenized by horizontal mixing: the thinning of the layer as one moves offshore thus enhances a negative current shear, culminating in a maximum velocity at the outcrop. In the lower layer, the rectified flow is slightly intensified as one moves shoreward because of a sharper change in layer thickness, which however is countered by enhanced bottom friction that eventually weakens the flow to zero at the foot of the front. Since flow in the frontal zone is dominated by that in the upper layer, the combination of uniform PV in the upper layer and the thermal-wind relation would yield a width of the frontal zone given roughly by the baroclinic deformation radius (based on the anchoring depth). With an anchoring depth of about 0.3, this deformation radius is about 0.55 in dimensionless unit, which is consistent with the solution. In addition, the maximum surface flow at the outcrop should be scaled by f times that distance, or 0.55 when nondimensionalized, again in agreement with the solution. It should be emphasized that this velocity is mainly a function of stratification and anchoring depth, independent of the tidal amplitude or topographic slope, as is the case of a homogeneous ocean. The surface jet shown in Fig. 2 has a dimensional value of about 0.5 m s^{-1}, more than doubling the strength of the maximum flow of the unstratified ocean.

I have not attempted to solve for the cross-frontal circulation when subjected to rectified flux, but considering only Ekman transport associated with mean flow shown in Fig. 2, one expects a strong convergence at the foot of the front. Since Lagrangian mean flow may

differ significantly from the Eulerian mean flow (Loder and Wright 1985), a more involved study is needed to assess the particle trajectory or tracer dispersion. It is nevertheless significant that the mean along-isobath flow derived from the model tends to stiffen the front as a barrier to offshore (Eulerian) transport of water mass properties.

I have also calculated the solution when stratification and/or the anchoring position of the front have changed. These solutions are not shown since modification to Fig. 2 is quite trivial and consistent with what is to be expected from the above scaling arguments. For example, when stratification intensifies, the frontal zone would span over a wider zone, accompanied by a stronger surface jet. But since the baroclinic deformation radius varies as the square root of reduced gravity, the change is less than 50% even if stratification has increased by a factor of 2. The flow in the lower layer, being constrained to vanish at the foot of the front, has exhibited even smaller change. Similarly, if the anchor depth changes, the width of the frontal zone and the associated surface jet would change accordingly, and again not particularly strongly because of the square-root dependence on such depth. In practice, of course, stratification and the anchoring depth may not be independently varied, but likely to be coupled. In accordance with Simpson's criterion (Simpson and Hunter 1974), for example, a stronger stratification would be accompanied by a shallower anchoring depth so that their effects on the solution as discussed above tend to cancel, resulting in a solution less sensitive to individual variations. Some effects of varying α can be anticipated from discussions in Part I. For example, an increase in this parameter (say, due to a weaker tide) would reduce the overall magnitude of the mean flow that is in contact with the bottom. More subtly though, the reduced velocity difference across the bottom front would yield a flatter density interface just above the bottom boundary layer. As this may result in a wider frontal zone, one expects the maximum surface flow to be slightly enhanced.

Although I have neglected interfacial stress and mixing across the bottom front in calculating the solution, one may nevertheless deduce their effects on the solution based on vorticity balances (2.25) and (2.26). In the discussion following (2.25), note that interfacial stress tends to increase PV of both layers, which would render the lower layer flow just offshore of the frontal anchor slightly negative. Since, as discussed in connection with (2.26), mixing across the bottom front also adds positive PV to the inshore water, it augments the interfacial stress in weakening the mean flow just inshore of the bottom front. These changes in the flow on two sides of the bottom front would flatten the front, which would then span a slightly wider zone.

4. Discussion

As stated earlier, the intention of the model is to extend the diffusivity solution of a homogeneous ocean

discussed in Part I to the case when there is a density front. As the latter is taken as a given fact and moreover approximated as a density discontinuity, the model obviously cannot address frontogenesis processes or the associated cross-frontal circulation. The effect of these and other neglected processes may significantly modify the solution, especially where tidal diffusivity (a function of tidal amplitude) is small. While we have discussed the solution behavior in response to isolated changes of ''external'' parameters, it should be noted that these parameters are likely coupled through balances not considered in the model, one thus may not be sure about the aggregate behavior of the front. In any event, such deliberation may not have much practical value since the front is highly variable, subject to other forcing and hydrodynamic instabilities. The main utility of the model is to underscore dynamical closure of the system, and the particular solution shown in Fig. 2 suffices to reveal the first-order effect of a front on a tidally rectified flow.

We have considered here only a bottom-to-surface front, but over Georges Bank, there is a thermocline offshore during the stratified season, and the front is typically characterized by shoreward branching of that thermocline, which intersects both top and bottom surfaces. While the frontal system is substantially more complicated, the basic closure can be similarly formulated. Based on physical discussion provided here, many qualitative properties of the solution can also be inferred. For example, since the mixing across the surface front now tends to increase—rather than decrease—PV of the inshore water, one expects a weaker flow inshore of the frontal zone. The thinning of the inshore water mass sandwiched between the two frontal interfaces again leads to a jet, but located at the wedge where the two branches adjoin, rather than at the surface. The PV mixing within the intruding surface layer from offshore actually causes a frontal jet that is directed in the opposite direction, which may or may not be a significant feature depending on frontal parameters. Because of the prevalence of such a frontal system, an extension of the present model maybe a worthwhile effort.

REFERENCES

Brickman, D., and J. Loder, 1993: Energetics of the internal tide on northern Georges Bank. *J. Phys. Oceanogr.,* **23,** 409–424.

Butman, B., and Coauthors, 1982: Recent observations of the mean circulation on Georges Bank. *J. Phys. Oceanogr.,* **12,** 569–591.

Chen, C., and R. C. Beardsley, 1995: A numerical study of stratified tidal rectification over finite-amplitude banks. Part I: Symmetric banks. *J. Phys. Oceanogr.,* **25,** 2090–2110.

Csanady, G. T., 1971: On the equilibrium shape of the thermocline in a shore zone. *J. Phys. Oceanogr.,* **1,** 263–270.

——, 1982: *Circulation in the Coastal Ocean.* D. Reidel, 279 pp.

Houghton, R., 1997: Lagrangian flow at the foot of a shelfbreak front using a dye tracer injected into the bottom boundary layer. *Geophys. Res. Lett.,* **24,** 2035–2038.

Loder, J. W., 1980: Topographic rectification of tidal currents on the sides of Georges Bank. *J. Phys. Oceanogr.,* **10,** 1399–1416.

——, and D. G. Wright, 1985: Tidal rectification and frontal circulation on the sides of Georges Bank. *J. Mar. Res.,* **43,** 581–604.

Magnell, B. A., S. L. Spiegel, R. I. Scarlet, and J. B. Andrews, 1980: The relationship of tidal and low-frequency currents on the north slope of Georges Bank. *J. Phys. Oceanogr.,* **10,** 1200–1212.

Namie, C. E., 1996: Georges Bank residual circulation during weak and strong stratification periods: Prognostic numerical model results. *J. Geophys. Res.,* **101,** 6469–6486.

Ou, H. W., 1999: A model of tidal rectification by potential vorticity mixing. Part I: Homogeneous ocean. *J. Phys. Oceanogr.,* **29,** 821–827.

Simpson, J. H., and J. R. Hunter, 1974: Fronts in the Irish Sea. *Nature,* **250,** 404–406.